Incremental distribution of strontium and zinc in great ape and fossil hominin cementum using synchrotron X-ray fluorescence mapping

Christopher Dean[1], Adeline Le Cabec[2], Kathryn Spiers[3], Yi Zhang[3], Jan Garrevoet[3]

[1]Department of Cell and Developmental Biology, University College London, Gower Street, London, WC1E 6BT, UK
[2]Department of Human Evolution, Max Planck Institute for Evolutionary Anthropology, Deutscher Platz 6, D-04103 Leipzig, Germany
[3]Deutsches Elektronen-Synchrotron DESY, Notkestraße 85, 22607 Hamburg, Germany

Subject Category:
Life Sciences – Physics interface

Subject Areas:
Biophysics, evolution

Author for correspondence:
Christopher Dean
Email: ucgacrd@ucl.ac.uk

Abstract

Cementum and the incremental markings it contains have been widely studied as a means of ageing animals and retrieving information about diet and nutrition. The distribution of trace elements in great ape and fossil hominin cementum have not been studied previously. Synchrotron X-ray fluorescence (SXRF) enables rapid scanning of large tissue areas with high resolution of elemental distributions. First we used SXRF to map calcium, phosphorus, strontium and zinc distributions in great ape dentine and cementum. At higher resolution we compared zinc and strontium distributions in cellular and acellular cementum in regions where clear incremental markings were expressed. We then mapped trace element distributions in fossil hominin dentine and cementum from the 1.55-1.65 million year old site of Koobi Fora, Kenya. Zinc in particular is a precise marker of cementum increments in great apes, and is retained in fossil hominin cementum, but does not correspond well with the more diffuse fluctuations observed in strontium distribution. Cementum is unusual among mineralised tissues in retaining so much zinc. This is known to reduce the acid solubility of hydroxyapatite and so may confer resistance to resorption by osteoclasts in the dynamic remodelling environment of the periodontal ligament and alveolar bone.

Keywords:
Cementum, teeth, SRXF, great apes, human evolution

Running title: Zinc and strontium in cementum

1. Introduction

Teeth consist of a dentine core that contains a central pulp, or nerve, chamber. An enamel cap covers the crown of the dentine core and a thin layer of cementum covers the dentine root surface (figure 1). Cementum is an integral component of the periodontium, the structures that support, suspend and protect the tooth in its bony socket [1]. The periodontal ligament (PDL) contains principal collagen fibre bundles that run between the alveolar bone and the tooth root surface forming a ligamentous hammock-like attachment known as a gomphosis. The alveolar bone and PDL actively turnover and remodel throughout life as teeth erupt and move but the cementum covering the tooth root surface does not [2–4]. As layers of cementum mineralise over the root surface the extrinsic collagen fibres of the PDL become embedded within it where they are known as Sharpey's fibres (figure 1). The environmental interface between the PDL and cementum surface must both prevent the PDL from mineralising and control the rate and extent of cementum formation [5]. Cementum also resists resorption more than alveolar bone when, for example, teeth move in response to pressure, such as during orthodontic treatment [6,7]. Root dentine not covered with cementum tends to undergo resorption [8]. New layers of cementum are added in a regular incremental manner (figure 1) and act as a barrier to limit the down-growth of gingival epithelium and resulting loss of PDL attachment [9]. Each layer also sequesters a rich matrix of growth factors that can be released to induce PDL regeneration when needed [9,10].

In cementum forming over the first-formed two thirds of the root, mineralised Sharpey's fibres cover as much as 100% of the cementum surface but their cores may remain unmineralised [11]. In the last-formed cementum around the root apex Sharpey's fibres only occupy 40-60% of the cementum surface [11]. Where there is space between the larger 3-12 μm diameter Sharpey's fibres, smaller intrinsic collagen fibres (1-2 μm diameter) formed by cementoblasts weave between them running parallel to the root surface [6,12]. Cementum around the root apex starts to form after the time a tooth reaches functional occlusion [13]. It responds to tooth movement such as tipping and eruption as the tooth crown wears away by laying down layers of cementum in a compensatory way [4,14,15]. Rates of apical cementum formation are typically greater, which together with the multipolar nature of the cementoblasts in this region that can secrete matrix on any aspect, is thought to result in cementoblasts becoming incorporated into the growing apical cellular cementum.

1.1 Incremental markings in cementum

The nature of the incremental markings in both acellular cementum and cellular cementum is complicated. Demineralised and stained thin sections of cementum [see figures 11.2 and 11.13 in 7] demonstrate that even the unmineralised organic cementum matrix contains incremental markings visible within it. Biglycan is associated with incremental markings in cellular cementum and along with other glycosaminoglycans (decorin, lumican, and versican) is associated with cellular but not acellular cementum growth [9,16]. Cementoblasts forming acellular cementum exert much stricter regulation of local inorganic pyrophosphate levels than cementoblasts forming cellular cementum, which has a profound influence on rates of mineralisation [5]. There is growing evidence that acellular cementum and cellular cementum may be formed from different cementocyte populations of different origins with different phenotypes [7,8,13]. Cementoblasts forming acellular cementum

derived from, or influenced by, the epithelial root sheath express, for example, cytokeratin but not osteocalcin, parathormone receptors, TGF-beta and IGF, whereas the reverse is true of cementoblasts of possible mesenchymal origin forming cellular cementum [7,13].

The principal inorganic component of cementum is hydroxyapatite and represents ~65% of its wet weight. The crystals in cementum measure 55 nm wide by 8 nm thick [7] although tricalcium phosphate, octacalcium phosphate and carbonated hydroxyapatite [of type B substitution, see 17] are also present [18,19]. Alternating light and dark bands, about 2.5 μm thick [12] seen in undemineralised ground sections of teeth in transmitted light microscopy (TLM) correspond with alternating levels of mineralisation. Dark bands are thought to correspond with slower forming cementum, and light bands with faster forming cementum but which bands are more or less mineralised remains unclear [15,18–20]. Using Raman polarised acquisitions, Colard et al. [18] have also observed better aligned collagen fibres within dark bands than in light bands, with mineral crystals always lying parallel to the collagen fibres. Lieberman [15] suggested nutritional status determines the rate of acellular cementum formation but also that changes to the magnitude and frequency of chewing forces underlie shifts in the orientation of the principal collagen fibres within the PDL that in turn determine the angle at which Sharpey's fibres become embedded within forming cementum [21]. Some or many of these aspects of cementum microstructure may be preserved in fossil teeth, as they are in fossil bone [22], and so potentially provide information about the diet and lifespan of extinct taxa.

1.2 Trace elements in cementum

Both barium and strontium are incorporated into growing tooth tissues but Ba levels are much lower [23-25] and typically <10 ppm rather than ~200 ppm for Sr. Recently, enriched regions of Ba in orang-utan teeth have been linked to concentrated levels in breast milk and Ba released from the maternal skeleton during periods of nutritional stress [23]. Strontium on the other hand is depleted in breast milk [24,25] but is known to mirror both background environmental levels and diet [26,27,28]. Strontium concentrations are higher in cementum (158 ppm) than in dentine [29]. Since cementum continues to grow incrementally over a lifetime, the distribution of Sr in great ape teeth may yet provide chronological information about diet, geographical location and even late nursing history. Nursing history and diet are extremely diverse among living great apes, especially between gorillas and orang utans in their natural habitats [23].

A number of studies have identified zinc in bone and dental tissues [19,22,28–35]. Overall, cementum is zinc-enriched (407 ppm) compared with dentine and bone [34]. Slow forming peritubular dentine is also zinc-rich [36,37] as is the forming mineral front in bone [32] which has prompted suggestions that Zn is elevated where mineralisation is active but also that high levels at the mineralising front itself may only be transient [37]. On this basis it has been predicted that Zn will be strongly concentrated at the cementum surface in all vertebrates with apatitic teeth [30]. Besides cementum, high Zn levels have been demonstrated in slow growing secondary dentine surrounding the pulp chamber [29–31] but it is not clear in either cementum or dentine if Zn substitutes largely for Ca in the hydroxyapatite lattice or is to some extent also retained in the non-collagenous protein matrix or both [37]. In a study of faster growing cellular cementum in Beluga whale teeth [30], Zn was found

to be the most sensitive indicator of changes in mineralisation. Peaks in Zn and Ca fluorescence intensity and in the carbonated hydroxyapatite diffraction intensity occurred together and corresponded with the bright bands visible in TLM. The same observations have been made in slower growing acellular cementum in human, reindeer, red deer and bovid cementum [19]. Indeed, it has been suggested Zn may provide a more reliable way of visualising cementum growth increments than TLM [30]. However, while there is some evidence for this in human, reindeer, red deer, bovid and Beluga whale cementum, there have been no studies of acellular or cellular cementum microstructure and chemistry in living great apes, nor has cementum microanatomy been routinely employed in studies of human evolution in the way it has in archaeology.

In this study we first mapped the general distribution of Sr and Zn at low resolution in *Pan*, *Gorilla* and *Pongo* incisors that grow for ~10 years and then mapped Ca, P, Sr and Zn in a region expressing especially well-defined acellular cementum increments in TLM. In this way any commonalities between those already reported in humans and other animals could be established. We then studied two regions of regular faster formed compensatory acellular cementum, that again expressed clear incremental markings in TLM, to describe Sr, Ca, P, and Zn distribution in the same specimens and to document their relationship to incremental growth markings at a greater resolution. Finally, we mapped the distribution of trace elements in a fossil hominin tooth root to investigate the effects of diagenesis and assess the potential for including cementum microanatomy and chemistry in future studies of human evolution.

2. Materials

It is a feature of humans, great apes, and fossil hominins with relatively long lifespans that with increasing age anterior teeth rotate or tip in a compensatory way in response to crown wear and/or continued eruption of the tooth and changing tongue and lip pressure [14,38]. Thick deposits of compensatory cellular cementum then often form on the lingual aspects of the tooth root apex. First, four old worn great ape central incisors from three individuals in the Elliot Smith Research Collection housed at University College London were chosen for this study: (*Pongo*, female, UCL-JS3-CA-28-UI1; *Gorilla*, male, UCL-CA1G-1474-UI1; *Pan,* female UCL-CA-14E-LI1 and UI1). These specimens were collected in the 1920's and were originally free-living in their natural habitats. Then a 1.55-1.65 million-year-old fossil hominin canine root attributed to *Paranthropus boisei* (KNM-ER 1817, from Koobi Fora, Kenya, [39–41]) with thick regularly formed apical compensatory cellular cementum was chosen.

3. Methods

3.1. Sample preparation

Teeth were sectioned longitudinally with a low speed diamond saw (*Buehler IsoMet*). One cut face was polished using a graded series of abrasive papers and finished with 3 μm aluminium polishing powder and deionised water on a polishing pad. This polished surface was cleaned in an ultrasonic bath, dried and then fixed to a 1 mm glass slide with zero-bond epoxy resin (*Huntsman Araldite 2020*) under pressure for 48 hours. A further cut was then made parallel with the glass slide and tooth block leaving a 300-400 μm thick longitudinal tooth section attached to the slide. This was then ground and lapped to between 80-100 μm and polished and mounted using *DPX*

(Distyrene, Phthalate plasticiser and Xylene) for TLM. Laser confocal (LC) micrographs and TLM micrographs were first made of regions of interest in the cellular cementum of the great ape specimens where incremental markings were well expressed and in KNM-ER 1817 where there was particularly good preservation of cementocyte lacunae and Sharpey's fibres. In this latter case a z-series of 75 individual confocal slices, each 0.2 μm thick, was averaged to depict one small area of cellular cementum with greater depth of field at high power (×50 objective). Following this, the great ape ground sections were then unmounted, by soaking in dimethylformanide for 2 to 3 days. Each thin section was then floated off the slide, cleaned dried and secured onto 50 μm thick kapton polyimide film strips with double-sided adhesive tape and mounted onto steel sample holders, centrally aligned within the SXRF scanning window. Care was taken to mount all plane-parallel polished samples perfectly flat on the sample holder to ensure true focus over the whole section. The ground section of KNM-ER 1817 was judged too fragile to remove from the glass slide and so only the glass coverslip and DPX mounting medium was removed by soaking in xylene. The specimen was then mounted directly onto the steel sample holder still attached to the glass slide.

3.2. Synchrotron X-ray Fluorescence (SXRF) and Diffraction (SXRD) setup

Experiments were performed on the Beamline P06 [42], Petra III, at DESY (Deutsches Elektronen-Synchrotron), Hamburg, Germany. The storage ring was operated in 40-bunch mode using top-up filling mode with a current of 100 mA ± 0.5 mA. The primary X-ray beam was monochromatised to 17.0 keV using a double crystal Si111 monochromator and focused using a Kirkpatrick-Baez (KB) mirror system (JTEC, Japan) to the size of 0.5 × 0.5 μm. The focused X-ray beam decreases the background signal, thus improving trace element sensitivity, in combination with a low radiation dose [43]. The set-up comprises an Eiger X 4M Detector (Dectris Ltd.) and a Maia detector system [44] which allows for large area SXRF imaging with a sub-micrometer resolution using millisecond dwell times [45]. The Maia detector is ideally used in 180° or "backscatter" geometry for thin samples (~100 μm-thick in this study). The sample is placed at an angle of 90° to the incident X-ray beam, beyond the Maia detector; see figure 2 in [43]. This allows for the simultaneous acquisition of X-ray diffraction (SXRD) data using a photon counting detector, the Eiger X 4M (Dectris Ltd.). The sample to detector distance used for diffraction pattern collection is 133.5 mm. The Maia Si detector wafer comprises 384 1 mm^2 diode elements arranged in a 20 × 20 array, with 4 × 4 elements missing in the centre of the detector and forming a hole to allow the incident beam to pass through. These dimensions, combined with close sample position, result in the detector wafer subtending a sample solid angle of approximately 1.3 sr. Data is acquired in 'flyscanning' mode by continuously moving the sample. Due to the short dwell times, dose deposition is kept to a minimum. The sample holder supporting the sample is fixed on the sample stage using a kinematic mount (Newport). Elements of primary interest were Ca, P, Sr, and Zn therefore the primary energy of 17 keV was chosen, sufficient to excite the Sr K-shell but not the Mo mask in the Maia detector. Spectral analysis, deconvolution and initial image analysis of the fluorescence data were performed using GeoPIXE 7.4f. Elemental distribution maps were normalised using the incoming X-ray flux. SXRF concentrations are reported as ppm (by weight). The SXRD data has been evaluated using software developed in-house based on the PyFAI library [46].

3.3. Data acquisition

Low resolution overview scans of whole hemi (buccal) incisor tooth roots were first acquired with a resolution of 25 μm, and an integration time of 25 ms. Scans of the lingual half of the root (dentine and part of the pulp cavity) and cementum were made for each of the four great ape teeth and of the preserved distal root portion of the KNM-ER 1817 canine. Three specific regions of interest, identified with TLM as having exceptionally well defined incremental markings, were then scanned at higher resolution to visualise fine cementum microstructures. This was done at either 1 or 5 μm resolution and 10 or 25 ms of integration time according to a trade-off between scan-area and scan-time for each field of view. Region 1 was of acellular cementum in the midroot of *Pongo*, UCL-JS3-CA-28-UI1 (green bounding box, figure 2a). Region 2 was of regular compensatory cellular cementum at the apex of *Pan* UCL-CA-14E, UI1 (both regions at 5 μm). Region 3 was again of regular compensatory cellular cementum but in an opposing tooth from the same individual at the apex of *Pan* UCL-CA-14E, LI1 and was scanned at 1 μm resolution where incremental lines were maximally spaced apart. Regions 2 and 3 were both on the lingual aspects of the *Pan* incisor teeth UCL-CA-14E UI1 and UCL-CA-14E LI1 and so are not shown in figure 2. There were no regions within the *Gorilla* cementum with especially well defined incremental growth markings.

4. Results

Overview maps (resolution: 25 μm) showing Sr and Zn distributions within the buccal incisor root dentine and cementum are shown in figure 2. In all cases the growing roots have incorporated Sr into both primary and secondary dentine in a pattern that follows the incremental root dentine growth lines. However, the concentration of Sr varies greatly. There are alternating but irregularly distributed regions of Sr depletion and Sr enrichment within each root. Zn distribution is different and largely limited to the slow-formed secondary dentine surrounding the pulp chamber and to the cementum on the root surface.

4.1. Region 1; acellular cementum in the midroot of *Pongo*, UCL-JS3-CA-28-UI1

Acellular cementum (figure 3) appears generally to be more mineralised than dentine. There is very little evidence of a gradient in Ca, Sr, Zn, or P concentration between the CDJ and the cementum surface in this region. Calcium concentration remains almost constant at 300,000 ppm and P at 150,000 ppm through the whole thickness of the cementum (figure 3e). Sharpey's fibres within acellular cementum are also especially well distinguished in the Ca map by their hypocalcified cores running at right angles from the CDJ to the cementum surface. Incremental markings are visible in the Ca map running parallel with the cementum surface and CDJ and measure 2-3 μm in width. These markings are faint in the P map, which appears almost uniform and homogenous in concentration across both dentine and cementum. Zinc occurs at highest concentration at the cementum surface (>2000 ppm but truncated in figure 3 at 450 ppm) and has a clear incremental distribution. Sr is also distributed in an incremental manner. In general there is poor correspondence between the minor fluctuations in Sr and Zn concentration and as far as can be resolved with Ca concentration. In excess of 25 incremental lines could be counted within the acellular cementum of this specimen.

4.2. Region 2; cellular cementum at the apex of *Pan* UCL-CA-14E, UI1

In figure 4d the green box over the Zn map depicts the plane orthogonal to the incremental markings of the concentration plots. As in Region 1 cellular cementum is not well distinguished from dentine by Ca concentration at the CDJ (figure 4a). There is a gradual Ca gradient from the CDJ (~220,000 ppm) to the cementum surface to 250,000 ppm but overall these values are slightly less than those (275,000 ppm) in the acellular cementum of *Pongo,* UCL-JS3-CA-28_UI1 (figure 3e). There is, however, less evidence of an accompanying gradient in P concentration across cellular cementum in Region 2 that remains constant at ~130,000 ppm (figure 4f). Zinc concentration shows a marked rise from ~75 ppm in dentine to ~150 ppm in cementum at the CDJ. However, Sr concentration fluctuates around ~225 ppm throughout. Clear regions of Sr enrichment and depletion exist in dentine and are distributed according to the incremental growth pattern of forming dentine. The cementum surface in this specimen appears both Sr and Zn rich with respect to the cementum generally. Peaks and troughs of Sr and Zn concentrations track each other quite tightly through the thickness of the cementum but there are places where they are out of phase with reciprocal concentrations (arrows in figure 4e).

4.3. Region 3; cellular cementum at the apex of *Pan* UCL-CA-14E, LI1

Figure 5 illustrates a 0.574 × 0.858 mm² region of cellular cementum from the opposing tooth of the same specimen as figure 4. The Ca map shows the plane (green bar) orthogonal to the incremental markings depicted in the concentration plots in figure 5b. With more widely spaced incremental markings and at higher resolution (1 μm) it is possible to better define the elemental contributions to the incremental markings visible in TLM. The TLM (figure 5a) shows regular incremental bright lines in the cellular cementum of this specimen (see also electronic supplementary material figures S1-6). These appear to have less well-defined Sharpey's fibres within them, perhaps reflecting greater mineral content.

Cementocyte lacunae and unmineralised, or hypomineralised, Sharpey's fibres are most easily visible in the Ca, P and Sr maps. Sharpey's fibres follow a sinuous course through the cellular cementum with some tending to change direction as they cross an incremental marking. Calcium concentration shows a slight peak at the CDJ (lower white arrows in figure 5a-5e) but there is less of a general gradient through the cellular cementum than in Region 2 (figure 4). Each incremental marking is associated with a slight rise in Ca concentration. Phosphorus concentration is more variable at ~115,000 ppm, slightly lower (~130,000 ppm) than in cellular cementum sampled in Region 2 (figure 4b) in the upper incisor, but from the same dentition, of *Pan* UCL-CA-14E. The P map shows only faint evidence of any incremental distribution (figure 5c). The bright lines in the TLM correspond closely with higher Zn concentrations (two examples are illustrated with white arrows in figure 5a-5e; see also electronic supplementary material figures S1-6). Zinc concentration fluctuates incrementally between 160,000 ppm to 300,000 ppm across the cementum. Zinc increments are fine, precise and well defined (figure 5e). Where Sr concentrations are high, they also correspond well with bright lines in the TLM but are more diffuse and sometimes span one or two cementum increments. While peaks in Zn concentration sometimes correspond with marked peaks in Sr concentration (figure 5f) there is generally poor correspondence between them. Zinc appears to be the best trace element proxy for the bright incremental markings visible in TLM [19,30]. Between

25 to 30 wider spaced cementum increments can be counted between the CDJ and the cementum surface in this Region 3. Notably, in both TLM and SXRF Ca, Zn, and Sr maps of cellular cementum there are additional finer closely spaced second order regular incremental markings between the more widely spaced increments. Where they can be counted there are ~12 between adjacent wider spaced cementum increments (figure 5a and 5b).

4.4. Fossil dentine and cementum in KNM-ER 1817

The TLM of the fossil canine root section (KNM-ER 1817) reveals good preservation of the dentine and cementum microstructure. Laser confocal images of the region depicted by the red box in figure 6a show empty air-filled spaces representing the unmineralised cores of Sharpey's fibres and cementocyte lacunae (backscattered light appears bright in the image). The incremental bands are not well defined but there is evidence for changing orientation of the Sharpey's fibres as they run a sinuous course across them. At higher power, cementocyte canaliculi can be imaged among the Sharpey's fibres with some suggestion of interconnections between them (figure 6c). The diagenetic changes in this fossil include very high concentrations of Ca (~400,000 ppm) where the cementum and dentine are now hypercalcified (figures 7 and 8). The pulp cavity, PDL space and cracks have become filled with calcite where Ca concentration reaches >450,000 ppm. The Fe distribution map also suggests surfaces, probably exposed to ground water, have accumulated greater concentrations of iron. Strontium in this tooth is more uniformly distributed in the cementum and dentine and appears to have risen in concentration in dentine and cementum to ~3,000 to 4,000 ppm in concert with Ca increase suggesting that any prior regions of relative Sr enrichment or depletion are now smothered and overprinted by Sr influx (figures 8 and 9). Figure 7e shows the distribution of apatite determined here by SXRD. Previous studies of this specimen have shown that while fluorapatite certainly substitutes for hydroxyapatite, some biological apatite remains, more in bone and dentine than in cementum [39,40]. Zinc concentration, however, remains distributed as it might have been in life at ~140 ppm, confined to the cementum and secondary dentine suggesting that Zn has not been lost or substituted and that some at least remains stable within the apatite lattice. Within cementum Zn still distributes incrementally (figures 8 and 9) and 20 to 25 incremental markings can be counted in some places.

5. Discussion

The low power distribution maps of Zn in *Pongo, Gorilla* and *Pan* incisors (figure 2) demonstrate that Zn levels are higher in slow-formed secondary dentine surrounding the pulp and in cementum covering the root surface. This confirms the findings of previous studies in humans and other animals [29-31,34]. The distribution maps for Sr in dentine and cementum (figure 2) also build on previous findings for modern humans [29]. Barium was not detected in this study, more than likely because the primary energy used of 17.0 keV was too low to excite electrons belonging to the Ba K-shell ($K\alpha$ = 32.194 keV). However, all four great ape incisors show evidence of strong alternating regions of Sr depletion and enrichment that follow the growth pattern of the dentine over ~10 years (figure 2a-e).

Strontium levels in mineralised hard tissues are thought to mirror physiological levels in tissue fluid [22,25], which in turn reflects geographical and geological location [26,27] and dietary intake, especially since some plants, nuts and fruits (and seafood)

concentrate Sr [47] and perhaps because dust from soil on vegetation and foodstuffs can vary between seasons. Strontium concentrations also depend upon the degree to which a cascade of metabolic processes discriminate against or favour Sr relative to Ca [25]. Specifically, Sr is excluded from breast-milk [24,25] and breast-feeding finishes long before 10 years of age in *Gorilla* and *Pan* when all incisor roots are completed but does continue for >8 years in *Pongo* [23] and so cannot, in *Pongo,* be discounted as an explanation for some regions of Sr depletion in incisor root dentine. These regions, however, would presumably coincide with regions of Ba enrichment [23]. It seems more likely, however, that fluctuation in Sr levels in great ape dentine and cementum would result from seasonal fluctuations in diet. That cementum potentially preserves a record of this over period of up to 20 or 30 years is significant for future retrospective studies of primate life history.

Acellular cementum in Region 1 from the mid-root region of the *Pongo* incisor (figure 3) again confirms the findings reported for acellular cementum in humans and other animals. The Ca, Zn and Sr maps all show evidence of incremental growth layers although the degree of correspondence between the peak concentrations of each element is poor. Both the maps for Zn together with the concentration plots for Zn (figures 3 and 4) confirm the prediction that Zn levels will be highest at the cementum surface where there was active ongoing mineralisation [30].

Closer direct contact with extra-cellular fluid [31] may not, however, be enough to explain the presence and distribution of Zn in cementum. In bone, Zn stimulates osteoblast proliferation, collagen synthesis and alkaline phosphatase activity [48] and the highest concentrations of Zn have been localised to growing Haversian bone surfaces where it co-distributes with alkaline phosphatase [32]. Alkaline phosphatase itself contains Zn and in cementum is involved in the tight regulation of cementum mineralisation by hydrolysing inorganic pyrophosphate (a potent inhibitor of hydroxyapatite formation). The presence of pyrophosphate is also one factor that ensures the PDL remains unmineralised [5]. Cementoblasts also regulate the thickness of cementum formed by controlling the transport of pyrophosphate from the intra- to the extra-cellular space through a protein (progressive ankylosis protein) but much more tightly in acellular cementum than in cellular cementum [5,49]. Zinc rich layers in cementum may then reflect either the initiation of bouts of mineralisation and/or proliferation and initiation of cementoblast secretory activity, or alternatively, regions of slower mineralisation where a greater amount of Zn from all sources is able to exchange with Ca over time.

Phosphorus concentrations in the acellular and cellular cementum (figures 3-5) studied here are remarkably constant and show little sign of incremental deposition. One reason for this may be that P exists not only in the hydroxyapatite component of dentine and cementum but also in their organic components whose distribution may be more homogenous. Moreover, the ratio of P to Ca differs in hydroxyapatite, calcium triphosphate and calcium octaphosphate each of which exist in cementum and dentine, as does amorphous Ca that might accumulate with age [17,18]. Here we show that Ca and P concentrations do not always co-vary in the same proportions in acellular and cellular cementum (figures 3e, 4f, 5g) nor can P concentrations be assumed to track gradients in Ca concentration through cementum.

An advantage of studying regularly formed compensatory cellular cementum in older primates is that it becomes easier to visualise the elemental distribution within incremental markings at higher resolution than in slower forming acellular cementum. Zinc distribution within cellular cementum studied here (figures 4, 5 and electronic supplementary material figures S1,S4), even at the low concentrations expected of trace elements, emerges as the clearest marker of incremental growth [19,30].

Higher resolution SXRF mapping of cellular cementum in Region 3 has revealed finer, second order, increments of growth between the wider spaced primary or first order increments (figure 5). Second order cementum increments have previously been described in female macaque monkeys where they were more numerous in male than female macaque monkeys [50]. However, the *Pongo* and *Pan* specimens in this study were both females and as an average of ~12 second order increments can be seen between what may be annular first order markings, this is perhaps suggestive of a monthly menstrual cycle being expressed in hominid cementum. Small physiological changes in blood pH and core temperature might well in theory influence mineralisation. Clearly, future studies on modern human and great ape material of known age with well-documented life histories are required to test this hypothesis, which for now remains speculative.

The diagenetic changes to both dentine and cementum of specimen KNM-ER 1817 may be very specific to the fossilisation process within the volcanic tuff deposits at Koobi Fora, Kenya. Nonetheless, the retention of Zn in fossil cementum and secondary dentine, raises hopes that Zn as a marker of cementum growth increments, might prove useful in future life history studies of early hominins especially from other fossil locations more favourable to trace element preservation [22]. Iron and calcite distribution on exposed surfaces and within cracks and fissures and even at higher resolution within the Sharpey's fibre spaces and cementocyte lacunae appear not to have penetrated the denser tissues (electronic supplementary material figures S7,S8). The preservation of air-filled spaces representing Sharpey's fibre orientation across the cementum layers in this fossil is excellent and suggests there were demonstrable shifts in diet during life [15,51]. Combining information for Sharpey's fibre orientation with Sr distribution in cementum may in the future shed light on how diet and/or geographical relocation changed through life among early fossil hominins.

5.1. Zinc as an adaptive component of cementum

Cementum appears to retain unusually high levels of Zn compared with other mineralised tissues where its presence during active mineralisation may be more transient [30]. Zinc readily substitutes for calcium in hydroxyapatite and confers greater resistance to acid dissolution [52–57]. Moreover, where Zn is present at concentrations >107 ppm, and at low pH (~4.0), it is actively involved in a dissolution/reprecipitation reaction where a new mineral phase (α-hopeite, α-$Zn_3(PO_4)_2.H_2O$) forms on the hydroxyapatite lattice surface, so blocking further demineralisation [58]. It follows that the ridges and troughs described from SEM micrographs on etched cementum surfaces [15,59 cited in 60] may be a reflection of alternating regions of high and low Zn concentration rather than, necessarily, greater and lesser levels of mineralisation generally. It is a property of cementum that it resists resorption in a dynamic environment where the PDL and alveolar bone are constantly remodelling in response to masticatory forces and tooth movements. Zinc both inhibits osteoclast cell formation and function [61,62] and reduces the acid

solubility of carbonated hydroxyapatite [52,53,58,63]. Moreover, in the slightly lower pH environment within the PDL that results from local interstitial ischaemia/hypoxia when, for example, consistent pressure is applied to teeth, this triggers osteoclast activity [64]. But it is alveolar bone that resorbs to enable tooth movement and migration and not cementum. Even when alveolar bone resorbs away around tooth roots leaving them exposed though fenestrations there is no apparent surface root resorption. Both Zn and to a lesser extent Sr substitutions in hydroxyapatite may, along with other factors [6,7], have a primary role in protecting tooth root cementum from resorption.

6. Conclusions

Cementum forms incrementally and accumulates over a lifetime. While Ca and P in hydroxyapatite predominate, trace elements are also incorporated into cementum. In great ape anterior teeth, faster forming regular compensatory cellular cementum resolves finer second order growth increments and a clear temporal record of Sr and Zn apposition. Changing diet and geographical location may underlie regions of Sr enrichment and depletion but Zn appears to mark either the initiation of bouts of mineralization, or alternatively, slower periods of cementogenesis. The bright growth lines visible in TLM coincide with peaks in mineral concentration but Zn lines may prove to be the best proxy for identifying and counting cementum annulations. Diagenetic changes to tooth tissues during fossilisation are many and complex [65,66] but cementum and secondary dentine still appear to retain Zn that distributes incrementally. Zinc may have an adaptive role in resisting resorption by osteoclasts.

Data accessibility. All experimental datasets are available from adeline_lecabec@eva.mpg.de
Author contributions. CD, JG, ALC conceived and designed the study. CD prepared the specimens. JG, KS, YZ CD, ALC, conducted the experiments. ALC, CD, JG, KS, YZ performed the analyses. CD, ALC, JG, KS wrote the manuscript. All authors gave final approval for publication.
Competing interests. The authors declare no competing interests.
Funding. This study was enabled by a project I-20160686 at Petra III, DESY, by lab support to CD from the Calleva Foundation and support to ALC from The Max Planck Society.
Acknowledgements. We thank the Government of Kenya and the National Museums of Kenya for continued access to precious fossil material in their care. We thank Drs Emma Mbua and Meave Leakey, Tim Arnett, Joanna Cameron, Jean-Jacques Hublin, the curators of the Elliot Smith Research Collection at University College London, the DESY User Office, Dr. Gerald Falkenberg, and those who have developed techniques employed in this study. Parts of this research were carried out at Petra III at DESY, a member of the Helmholtz Association (HGF). We thank three anonymous reviewers for their helpful comments.

References

[1] Cho M-I, Garant PR. Development and general structure of the periodontium. Periodontol 2000 2000;24:9–27. doi:10.1034/j.1600-0757.2000.2240102.x.
[2] Bosshardt DD, Selvig KA. Dental cementum: the dynamic tissue covering of the root. Periodontol 2000 1997;13:41–75. doi:10.1111/j.1600-0757.1997.tb00095.x.

[3] Nanci A, Bosshardt DD. Structure of periodontal tissues in health and disease. Periodontol 2000 2006;40:11–28. doi:10.1111/j.1600-0757.2005.00141.x.
[4] Marks SC, Schroeder HE. Tooth eruption: Theories and facts. Anat Rec 1996;245:374–93. doi:10.1002/(SICI)1097-0185(199606)245:2<374::AID-AR18>3.0.CO;2-M.
[5] Foster BL, Nagatomo KJ, Nociti FH Jr, Fong H, Dunn D, Tran AB, et al. Central Role of Pyrophosphate in Acellular Cementum Formation. PLOS ONE 2012;7:e38393. doi:10.1371/journal.pone.0038393.
[6] Jones SJ. Dental tissues: cement. In: Osborne JW, editor. Dent. Anat. Embryol., Oxford: Blackwell; 1981, p. 286–98.
[7] Berkovitz BKB, Holland GR, Moxham BJ, editors. Oral anatomy, histology and embryology. 5th edition. Edinburgh: Elsevier; 2018. ISBN 978-0-7234-3812-0
[8] Gonçalves PF, Sallum EA, Sallum AW, Casati MZ, Toledo S, Nociti Junior FH. Dental cementum reviewed: development, structure, composition, regeneration and potential functions. Braz J Oral Sci 2005;4:651–8. doi:10.20396/bjos.v4i12.8641790.
[9] Arzate H, Zeichner-David M, Mercado-Celis G. Cementum proteins: role in cementogenesis, biomineralization, periodontium formation and regeneration. Periodontol 2000 2015;67:211–33. doi:10.1111/prd.12062.
[10] Miki Y, Narayanan AS, Page RC. Mitogenic activity of cementum components to gingival fibroblasts. J Dent Res 1987;66:1399–403. doi:10.1177/00220345870660082301.
[11] Boyde A, Jones SJ. Scanning electron microscope studies of the formation of mineralized tissues. In: Slavkin HC, Bavetta LC, editors. Dev. Asp. Oral Biol. Academic press, New York, London: 1972, p. 243–74.
[12] Yamamoto T, Li M, Liu Z, Guo Y, Hasegawa T, Masuki H, et al. Histological review of the human cellular cementum with special reference to an alternating lamellar pattern. Odontology 2010;98:102–9. doi:10.1007/s10266-010-0134-3.
[13] Thomas HF. Root formation. Int J Dev Biol 1995;39:231–7.
[14] Villmoare B, Kuykendall K, Rae TC, Brimacombe CS. Continuous dental eruption identifies Sts 5 as the developmentally oldest fossil hominin and informs the taxonomy of *Australopithecus africanus*. J Hum Evol 2013;65:798–805. doi:10.1016/j.jhevol.2013.09.007.
[15] Lieberman DE. The Biological Basis for Seasonal Increments in Dental Cementum and Their Application to Archaeological Research. J Archaeol Sci 1994;21:525–39. doi:10.1006/jasc.1994.1052.
[16] Ababneh KT, Hall RC, Embery G. The proteoglycans of human cementum: immunohistochemical localization in healthy, periodontally involved and ageing teeth. J Periodontal Res 1999;34:87–96. doi:10.1111/j.1600-0765.1999.tb02227.x.
[17] Elliott JC. Structure, crystal chemistry and density of enamel apatites. In: Chadwick DJ, Cardew G, editors. Ciba Found. Symp. 205-Dent. Enamel, Chichester, UK: John Wiley & Sons, Ltd.; 1997, p. 54–72.
[18] Colard T, Falgayrac G, Bertrand B, Naji S, Devos O, Balsack C, et al. New Insights on the Composition and the Structure of the Acellular Extrinsic Fiber Cementum by Raman Analysis. PLoS ONE 2016;11:e0167316. doi:10.1371/journal.pone.0167316.
[19] Naji S, Rendu W, Gourichon L, Zhonghou CA, Stock S. Cementum ultrastructure, a comparative perspective from synchrotron X-ray scanning: fluorescence and diffraction. Am J Phys Anthropol 2017;162:296. doi:10.1002/ajpa.23210.

[20] Jones SJ. The root surface: an illustrated review of some scanning electron microscope studies. Scanning Microsc 1987;1:2003–18.
[21] Ho SP, Marshall SJ, Ryder MI, Marshall GW. The tooth attachment mechanism defined by structure, chemical composition and mechanical properties of collagen fibers in the periodontium. Biomaterials 2007;28:5238–45. doi:10.1016/j.biomaterials.2007.08.031.
[22] Anné J, Edwards NP, Wogelius RA, Tumarkin-Deratzian AR, Sellers WI, van Veelen A, et al. Synchrotron imaging reveals bone healing and remodelling strategies in extinct and extant vertebrates. J R Soc Interface 2014;11. doi:10.1098/rsif.2014.0277.
[23] Smith TM, Austin C, Hinde K, Vogel ER, Arora M. Cyclical nursing patterns in wild orangutans. Sci Adv 2017;3. doi:10.1126/sciadv.1601517.
[24] Humphrey LT, Dean MC, Jeffries TE, Penn M. Unlocking evidence of early diet from tooth enamel. Proc Natl Acad Sci 2008;105:6834–9. doi:10.1073/pnas.0711513105.
[25] Humphrey LT. Isotopic and trace element evidence of dietary transitions in early life. Ann Hum Biol 2014;41:348–57. doi:10.3109/03014460.2014.923939.
[26] Beard BL, Johnson CM. Strontium isotope composition of skeletal material can determine the birth place and geographic mobility of humans and animals. J Forensic Sci 2000;45:1049–61. doi:10.1520/JFS14829J.
[27] Britton K, Grimes V, Niven L, Steele TE, McPherron S, Soressi M, et al. Strontium isotope evidence for migration in late Pleistocene *Rangifer*: Implications for Neanderthal hunting strategies at the Middle Palaeolithic site of Jonzac, France. J Hum Evol 2011;61:176–85. doi:10.1016/j.jhevol.2011.03.004.
[28] Humphrey LT, Jeffries TE, Dean MC. Micro spatial distributions of lead and zinc in human deciduous tooth enamel. In: Irish JD, Nelson GC, editors. Tech. Appl. Dent. Anthropol., vol. 53, Cambridge: Cambridge University Press; 2008, p. 87–110.
[29] Martin RR, Naftel SJ, Nelson AJ, Feilen AB, Narvaez A. Synchrotron X-ray fluorescence and trace metals in the cementum rings of human teeth. J Environ Monit 2004;6:783–6. doi:10.1039/B408525F.
[30] Stock SR, Finney LA, Telser A, Maxey E, Vogt S, Okasinski JS. Cementum structure in Beluga whale teeth. Acta Biomater 2017;48:289–99. doi:10.1016/j.actbio.2016.11.015.
[31] Sánchez-Quevedo MC, Crespo PV, García JM, Campos A. X-ray histochemistry of zinc in dental tissues. Eur Arch Biol 1992;103:47–9.
[32] Gomez S, Rizzo R, Pozzi-Mucelli M, Bonucci E, Vittur F. Zinc mapping in bone tissues by histochemistry and synchrotron radiation–induced X-ray emission: correlation with the distribution of alkaline phosphatase. Bone 1999;25:33–8. doi:10.1016/S8756-3282(99)00102-7.
[33] Kang D, Amarasiriwardena D, Goodman AH. Application of laser ablation–inductively coupled plasma-mass spectrometry (LA–ICP–MS) to investigate trace metal spatial distributions in human tooth enamel and dentine growth layers and pulp. Anal Bioanal Chem 2004;378:1608–15. doi:10.1007/s00216-004-2504-6.
[34] Martin RR, Naftel SJ, Nelson AJ, III WDS. Comparison of the distributions of bromine, lead, and zinc in tooth and bone from an ancient Peruvian burial site by X-ray fluorescence. Can J Chem 2007;85:831–6. doi:10.1139/v07-100.
[35] Djomehri SI, Candell S, Case T, Browning A, Marshall GW, Yun W, et al. Mineral density volume gradients in normal and diseased human tissues. PLoS ONE 2015;10:e0121611. doi:10.1371/journal.pone.0121611.

[36] Stock SR, Veis A, Telser A, Cai Z. Near tubule and intertubular bovine dentin mapped at the 250 nm level. J Struct Biol 2011;176:203–11. doi:10.1016/j.jsb.2011.07.014.
[37] Stock SR, Deymier-Black AC, Veis A, Telser A, Lux E, Cai Z. Bovine and equine peritubular and intertubular dentin. Biomineralization 2014;10:3969–77. doi:10.1016/j.actbio.2014.05.027.
[38] Kaifu Y. Tooth wear and compensatory modification of the anterior dentoalveolar complex in humans. Am J Phys Anthropol 2000;111:369–92. doi:10.1002/(SICI)1096-8644(200003)111:3<369::AID-AJPA6>3.0.CO;2-#.
[39] Furseth Klinge R, Dean MC, Gunnaes A, Leakey MG. Microscopic structure and mineral distribution in tooth and periodontal tissues in a robust australopithecine fossil hominid from Koobi Fora, Kenya. In: Żądzińska E, editor. Curr. Trends Dent. Morphol. Res. 13th Int. Symp. Dent. Morphol., Wydawnictwo Uniwersytetu Lodzkiego Lodz, Poland: 2005, p. 233–42.
[40] Furseth Klinge R, Dean MC, Risnes S, Erambert M, Gunnaes AE. Preserved microstructure and mineral distribution in tooth and periodontal tissues in early fossil hominin material from Koobi Fora, Kenya. In: Koppe T, Meyer G, Alt KW, editors. Comp. Dent. Morphol., vol. 13, Karger Publishers; 2009, p. 30–5.
[41] Dean MC. Daily rates of dentine formation and root extension rates in *Paranthropus boisei*, KNM-ER 1817, from Koobi Fora, Kenya. In: Reynolds SC, Gallagher A, editors. Afr. Genes. Perspect. Hominin Evol., Cambridge: Cambridge University Press; 2012, p. 268–79.
[42] Schroer CG, Boye P, Feldkamp JM, Patommel J, Samberg D, Schropp A, et al. Hard X-ray nanoprobe at beamline P06 at PETRA III. X-Ray Mirror 2010;616:93–7. doi:10.1016/j.nima.2009.10.094.
[43] Sun Y, Gleber S-C, Jacobsen C, Kirz J, Vogt S. Optimizing detector geometry for trace element mapping by X-ray fluorescence. Ultramicroscopy 2015;152:44–56. doi:10.1016/j.ultramic.2014.12.014.
[44] Kirkham R, Dunn PA, Kuczewski AJ, Siddons DP, Dodanwela R, Moorhead GF, et al. The Maia Spectroscopy Detector System: Engineering for Integrated Pulse Capture, Low-Latency Scanning and Real-Time Processing. AIP Conf Proc 2010;1234:240–3. doi:10.1063/1.3463181.
[45] Falkenberg G, Fleissner G, Fleissner G, Alraun P, Boesenberg U, Spiers K. Large-scale high-resolution micro-XRF analysis of histological structures in the skin of the pigeon beak. X-Ray Spectrom 2017;46:467–73. doi:10.1002/xrs.2769.
[46] Ashiotis G, Deschildre A, Nawaz Z, Wright JP, Karkoulis D, Picca FE, et al. The fast azimuthal integration Python library: pyFAI. J Appl Crystallogr 2015;48:510–9. doi:10.1107/S1600576715004306.
[47] Bowen HJM, Dymond JA. Strontium and barium in plants and soils. Proc R Soc Lond B Biol Sci 1955;144:355–68. doi:10.1098/rspb.1955.0063.
[48] Seo H-J, Cho Y-E, Kim T, Shin H-I, Kwun I-S. Zinc may increase bone formation through stimulating cell proliferation, alkaline phosphatase activity and collagen synthesis in osteoblastic MC3T3-E1 cells. Nutr Res Pract 2010;4:356–61. doi:10.4162/nrp.2010.4.5.356.
[49] Foster BL. Methods for studying tooth root cementum by light microscopy. Int J Oral Sci 2012;4:119–28. doi:10.1038/ijos.2012.57.
[50] Kay RF, Cant JGH. 1988 Age assessment using cementum annulus counts and tooth wear in a free-ranging population of *Macaca mulatta*. *Am. J. Primatol.* **15**, 1–15. (doi:10.1002/ajp.1350150103)

[51] Lieberman DE. Life history variables preserved in dental cementum microstructure. Science 1993;261:1162-1164. doi:10.1126/science.8356448.
[52] Featherstone JDB, Nelson DGA. The effect of fluoride, zinc, strontium, magnesium and iron on the crystal-structural disorder in synthetic carbonated apatites. Aust J Chem 1980;33:2363–8. doi:10.1071/CH9802363.
[53] Crawford AW, De Bruin HJ. Concentration changes in surface Ca, P, F, Zn, Fe, and Sr during white spot formation. J Dent Res 1983;62:964–8. doi:10.1177/00220345830620091001.
[54] Tang Y, Chappell HF, Dove MT, Reeder RJ, Lee YJ. Zinc incorporation into hydroxylapatite. Biomaterials 2009;30:2864–72. doi:10.1016/j.biomaterials.2009.01.043.
[55] Curzon MEJ, Losee FL. Strontium content of enamel and dental caries. Caries Res 1977;11:321–6. doi:10.1159/000260286.
[56] Dedhiya MG, Young F, Higuchi WI. Mechanism for the retardation of the acid dissolution rate of hydroxyapatite by strontium. J Dent Res 1973;52:1097–109. doi:10.1177/00220345730520051901.
[57] Funato Y, Matsuda Y, Okuyama K, Yamamoto H, Komatsu H, Sano H. A new technique for analyzing trace element uptake by human enamel. Dent Mater J 2015;34:240–5. doi:10.4012/dmj.2014-127.
[58] Mohammed NR, Mneimne M, Hill RG, Al-Jawad M, Lynch RJM, Anderson P. Physical chemical effects of zinc on in vitro enamel demineralization. J Dent 2014;42:1096–104. doi:10.1016/j.jdent.2014.04.014.
[59] Hillson S. The scanning electron microscope and the study of ancient teeth. In: Olsen SL, editor. Scanning Electron Microsc. Archaeol., vol. 452, Oxford: British Archaeological Reports; 1988, p. 249–60.
[60] Burke A. Prey movements and settlement patterns during the Upper Palaeolithic in southwestern France. PhD Dissertation. New York University, 1992.
[61] Moonga BS, Dempster DW. Zinc is a potent inhibitor of osteoclastic bone resorption in vitro. J Bone Miner Res 1995;10:453–7. doi:10.1002/jbmr.5650100317.
[62] Yamaguchi M. Role of nutritional zinc in the prevention of osteoporosis. Mol Cell Biochem 2010;338:241–54. doi:10.1007/s11010-009-0358-0.
[63] Mayer I, Apfelbaum F, Featherstone JDB. Zinc ions in synthetic carbonated hydroxyapatites. Arch Oral Biol 1994;39:87–90. doi:10.1016/0003-9969(94)90040-X.
[64] Arnett TR. Acidosis, hypoxia and bone. Arch Biochem Biophys 2010;503:103–9. doi:10.1016/j.abb.2010.07.021.
[65] Stutz AJ. Polarizing microscopy identification of chemical diagenesis in archaeological cementum. J Archaeol Sci 2002;29:1327–1347. doi:10.1006/jasc.2001.0805.
[66] Trueman CN, Tuross N. Trace elements in recent and fossil bone apatite. Reviews in mineralogy and geochemistry 2002;48:489-521. doi:https://doi.org/10.2138/rmg.2002.48.13.

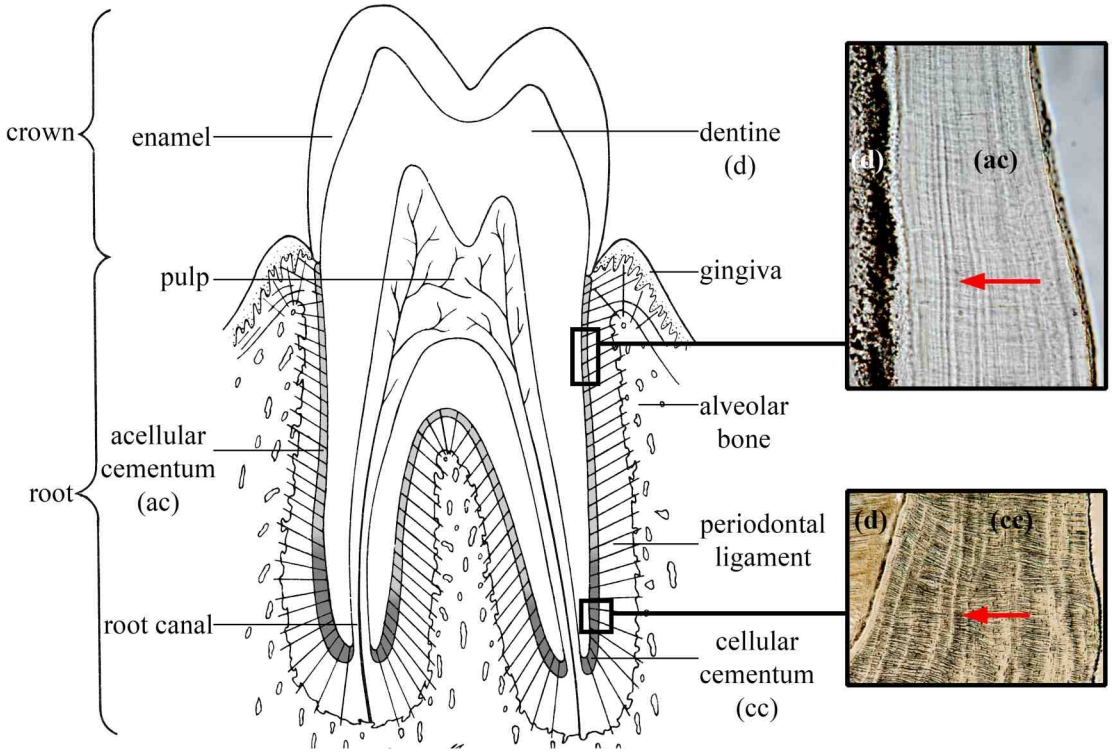

Figure 1
The tissue components of a tooth and periodontium showing the location of acellular (ac) and cellular cementum (cc) on the surface of the root dentine (d). Red arrows within boxes show the direction of extrinsic fibres, more prominent in (cc), also known as Sharpey's fibres. Bright incremental markings in both (ac) and (cc) run near-vertically.

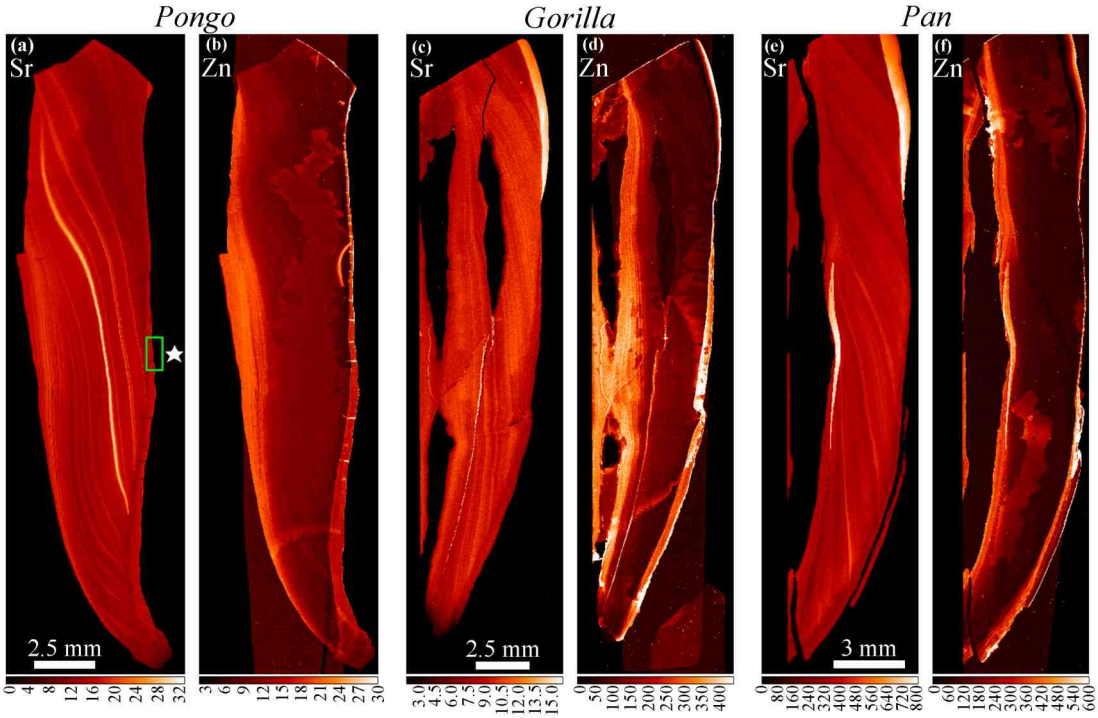

Figure 2
Overview SXRF scans (25 µm) of Sr and Zn distribution in the incisor tooth roots of *Pongo* (UCL-JS3-CA-28-UI1)*, Gorilla* (UCL-CA1G-1474-UI1) and *Pan* (UCL-CA-14E-LI1). Secondary dentine (on the pulpal aspect of each root) is to the left of each pair of images and cementum (on the root surface) to the right of each pair. Sr concentration (a), (c), (e) is extremely variable but generally follows the incremental growth pattern of root dentine. Zinc concentration (b), (d), (f), is highest in the secondary dentine surrounding the pulp cavity and in the cementum layers. The region highlighted by the green box in (a) in the Sr map (★) identifies regular compensatory acellular cementum scanned at 5 µm shown in Figure 3.

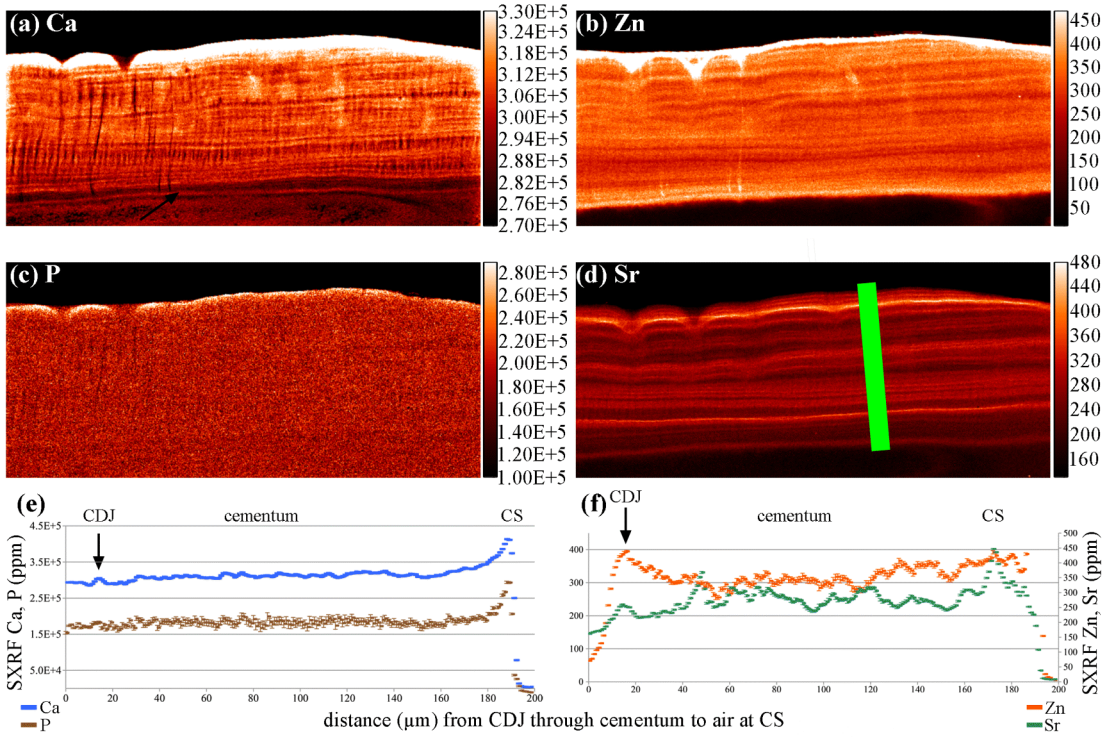

Figure 3
SXRF scans (1 µm) of Ca, P, Zn and Sr distribution in acellular cementum (a) to (d) respectively on the buccal aspect the upper incisor root of *Pongo* (UCL-JS3-CA-28). Black arrow indicated the first highly mineralised layer of cementum at the CDJ. Plots of SXRF Sr and Zn concentrations (ppm) are in the plane of the green bar (200 µm long) from the (CDJ) to the cementum surface (CS). There is poor correspondence of Zn and Sr levels. Values at the cementum surface reached 2284 ppm but were truncated above 450 ppm.

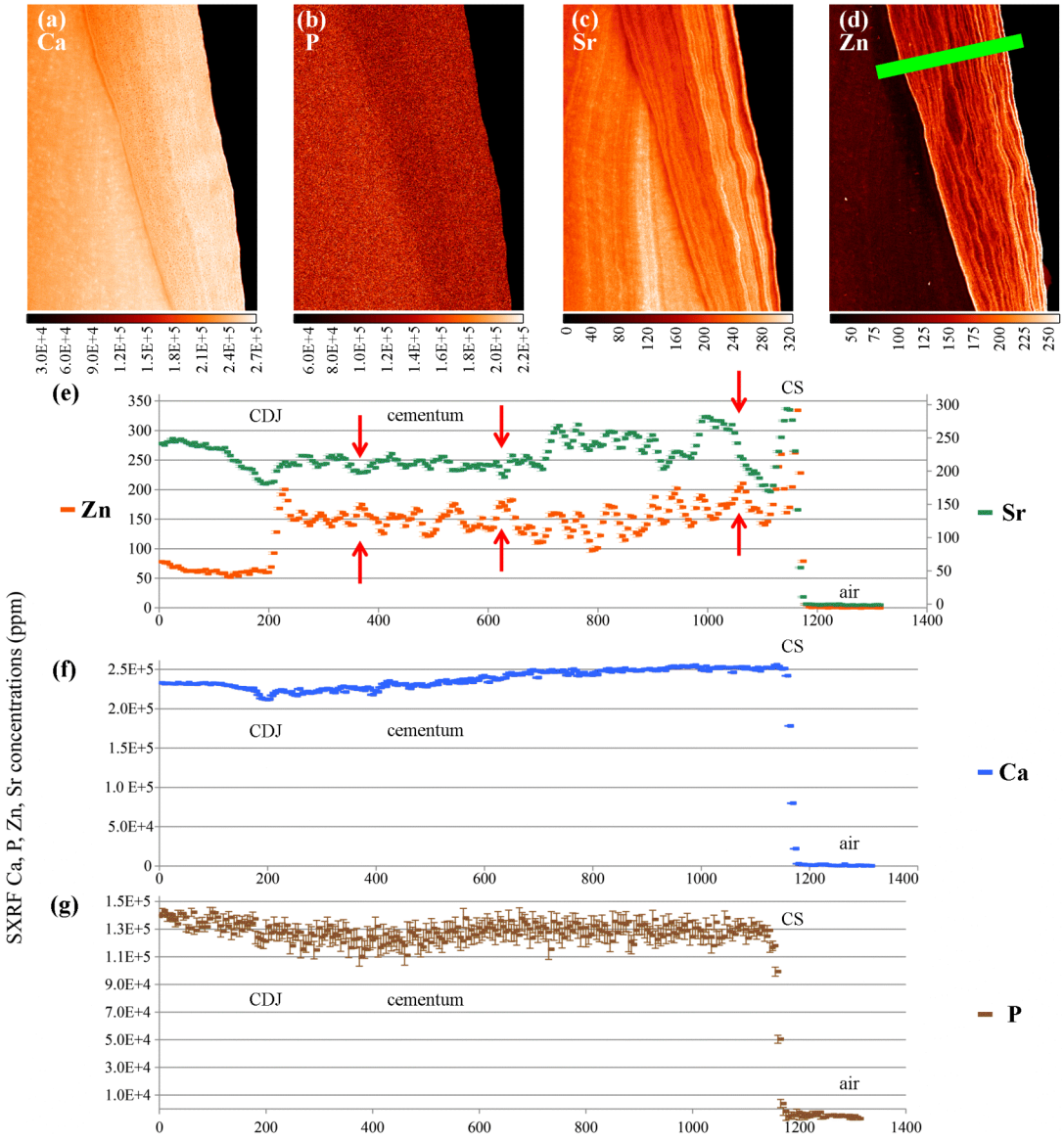

Figure 4
SXRF scans (5 µm) of Ca, P, Sr and Zn in a region of regular compensatory cellular cementum in the upper incisor root of *Pan* (UCL-CA-14E). The green bar (1350 µm long) on the Zn map (d) indicates the plane of SXRF Ca, P, Zn and Sr concentrations (ppm) plots. The red arrows in (e) show regions where Zn and Sr concentrations are reciprocal. Colour scales beneath each image denote concentration (ppm).

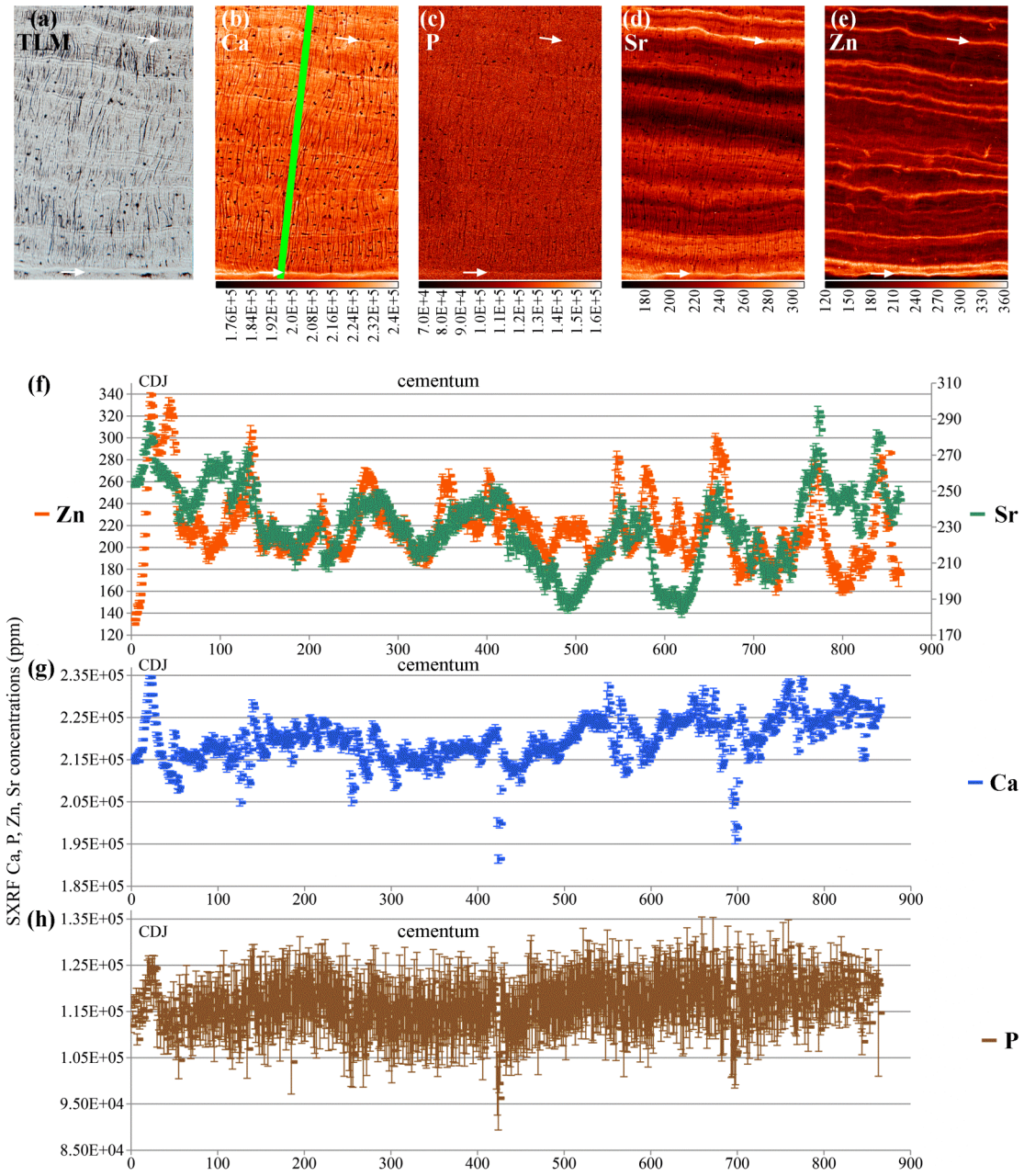

Figure 5
SXRF scans (1 µm) of Ca, P, Sr and Zn in regular compensatory cellular cementum in the lower incisor root of *Pan* (UCL-CA-14E) with the corresponding TLM on the left. The lower white arrows denote the first formed bright (dense) cementum layer at the CDJ. The upper white arrow denotes another clear bright marking in the TLM. The green bar (860 µm long) on the Ca map indicates the plane of SXRF Zn, Sr and Ca, P concentrations (ppm) plots. There is poor correspondence between Zn and Sr levels. Colour scales beneath each image denote concentration (ppm).

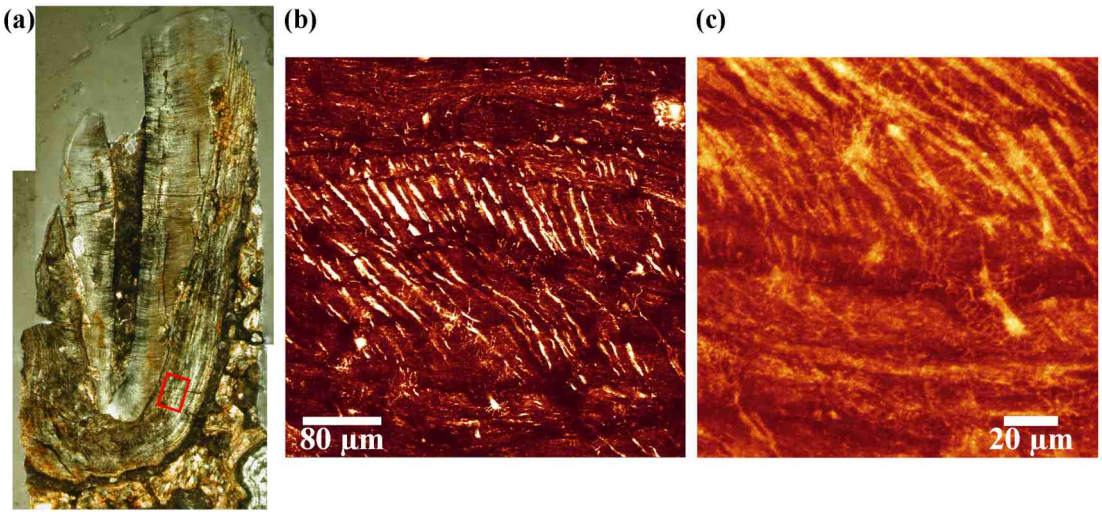

Figure 6
TLM (a) of canine root of KNM-ER 1817. Laser confocal image (b) of cementum layers, taken within the region of the red box. The right border of the red box is the lower border of the middle and right fields of view. Air-filled Sharpey's fibre spaces change orientation as they cross cementum layers. At higher magnification cementocyte lacunae and their canaliculi can also be imaged in this fossil (c).

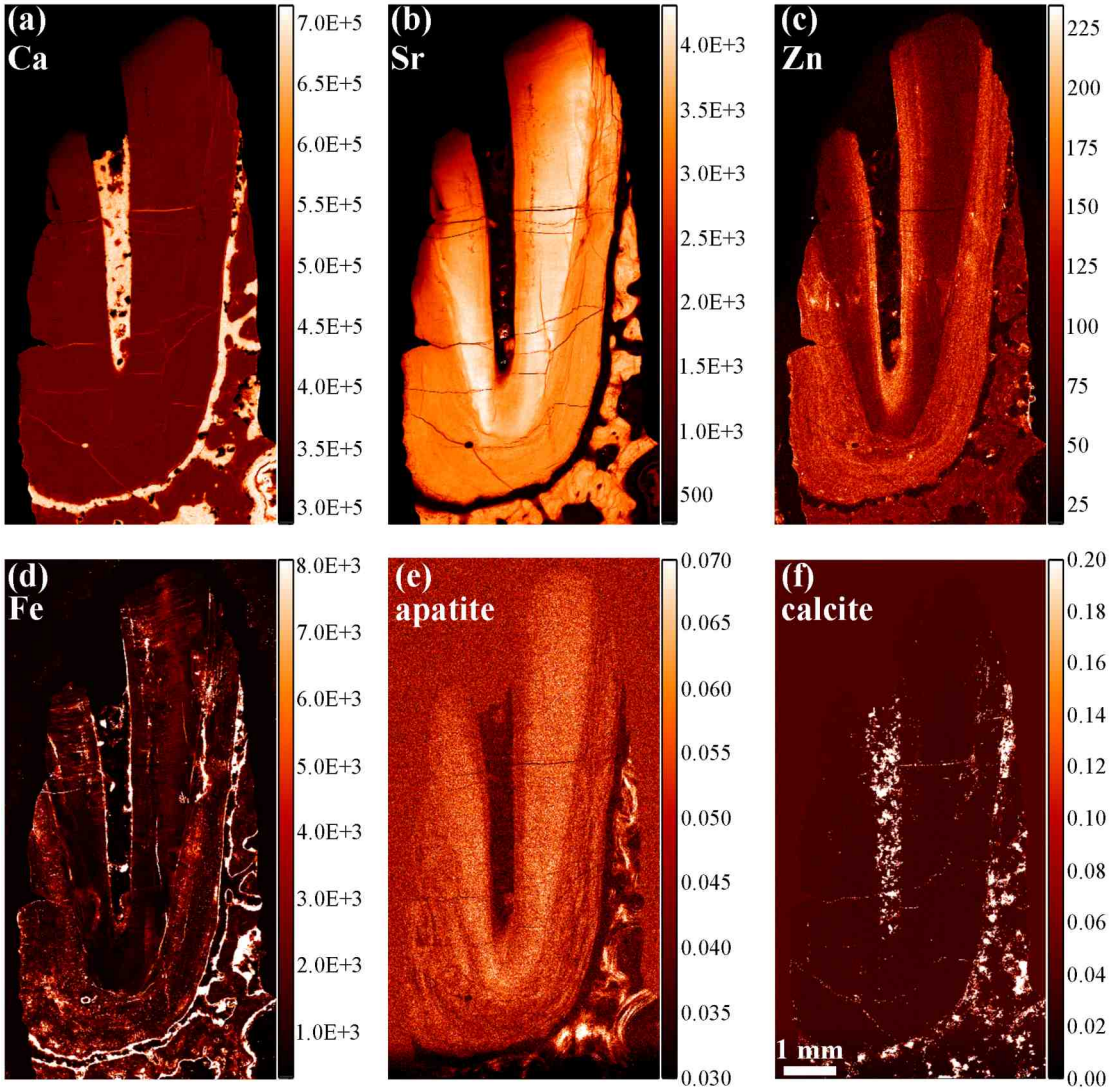

Figure 7
Overview SXRF maps of Ca, Sr, Zn and Fe distribution, (a) to (d) respectively, with overview SXRD images of apatite (e) and calcite (f) distributions in KNM-ER 1817. SXRF colour scales denote concentration (ppm) and SXRD scales relative intensity (a.u.).

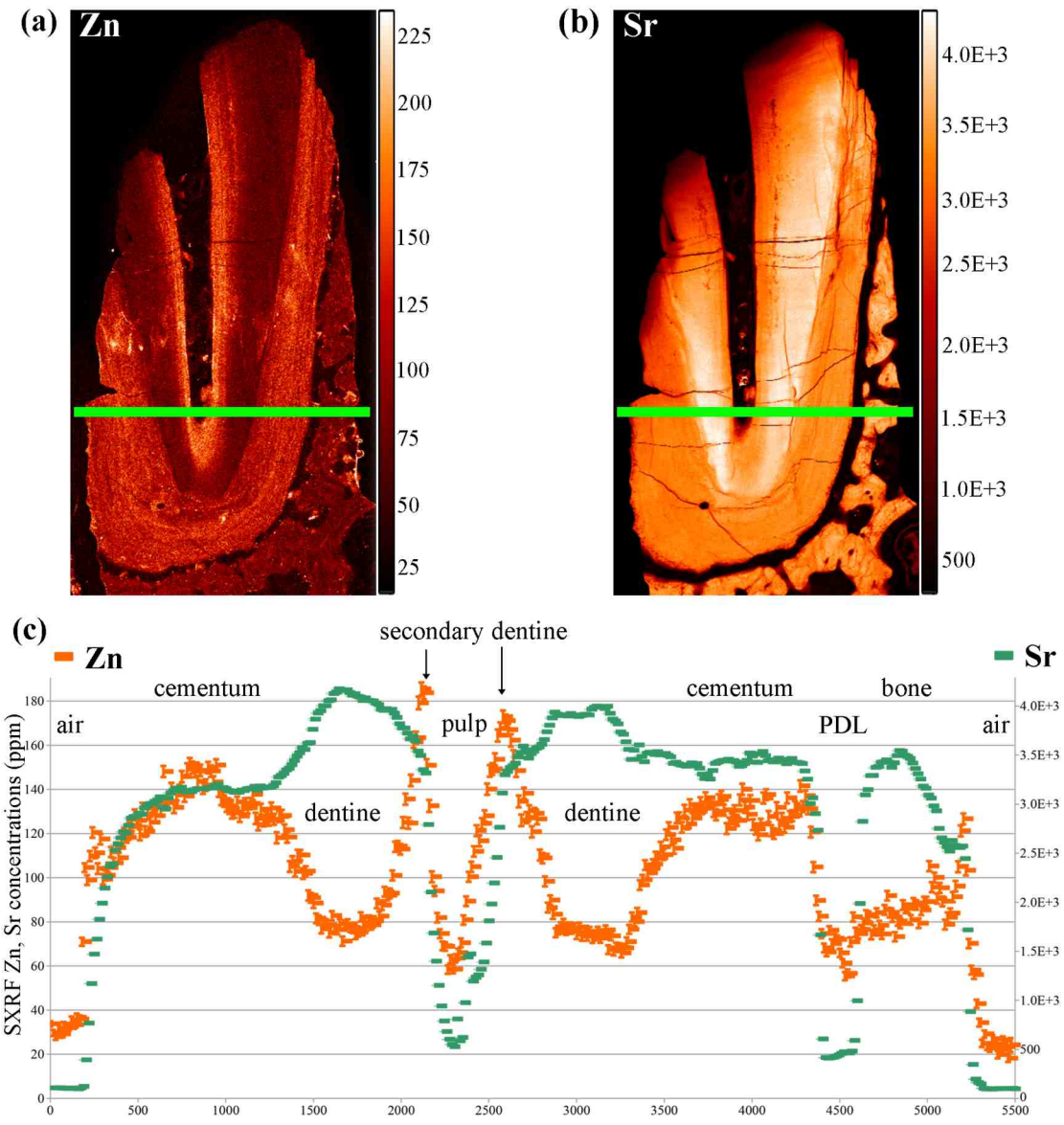

Figure 8
SXRF maps of zinc (a) and strontium (b) distribution in fossilised root dentine and cementum of KNM-ER 1817 (15 µm resolution). Plots (c) show Zn levels rising in cementum and in secondary dentine. Both Sr and Zn levels fall to near-zero in air, the pulp space and periodontal ligament space, both now filled of calcite. Colour scales alongside each image denote concentration (ppm).

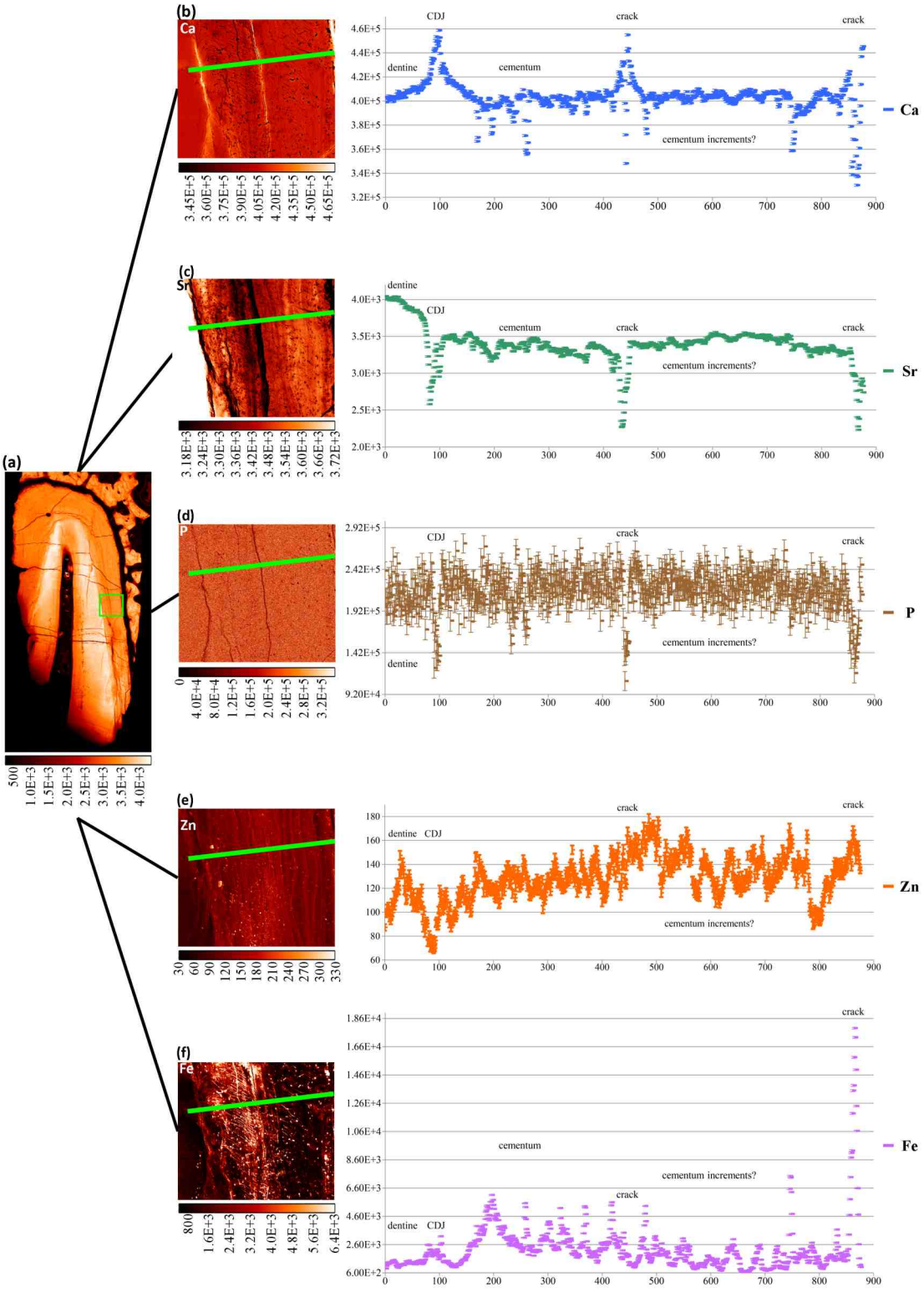

Figure 9
SXRF map of Sr in KNM-ER 1817 at 15 µm resolution (a) with green boundary box representing the location of SXRF maps of Ca (b), Sr (c), P (d), Zn (e) and Fe (f) at 1 µm resolution. Plots show Ca and Fe levels rise in the calcite containing cracks but P, Sr and Zn levels in cracks fall to very low levels. Fluctuations in Ca, P and Sr levels may correspond with cementum increments visible in the transmitted light micrograph (figure 6a). Colour scales beneath each image denote concentration (ppm).

Supplementary figures from **Incremental distribution of strontium and zinc in great ape and fossil hominin cementum using synchrotron X-ray fluorescence mapping.**

Christopher Dean, Adeline Le Cabec, Kathryn Spiers, Yi Zhang, Jan Garrevoet

Journal of the Royal Society Interface

Dated: December 10th, 2017

Figure S1

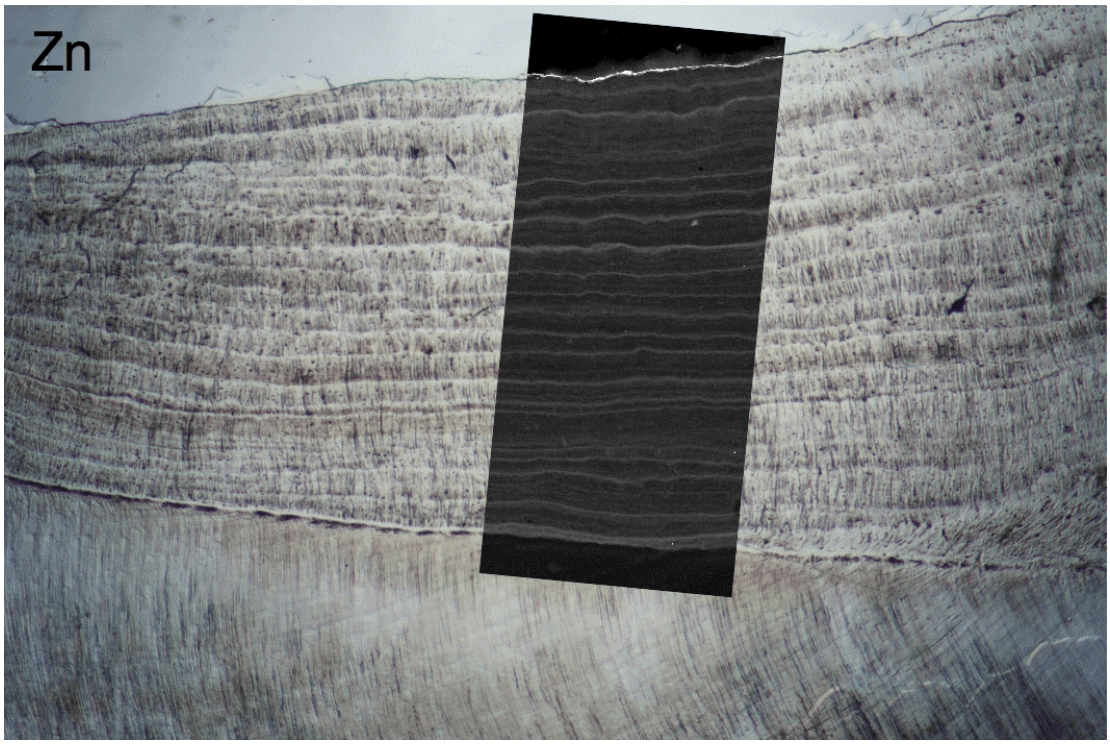

Zinc in *Pan* cellular cementum. Transmission light micrograph of cellular cementum in *Pan* (UCL CA14E LI1) overlain with SXRF map of zinc distribution (5 μm resolution).

Figure S2

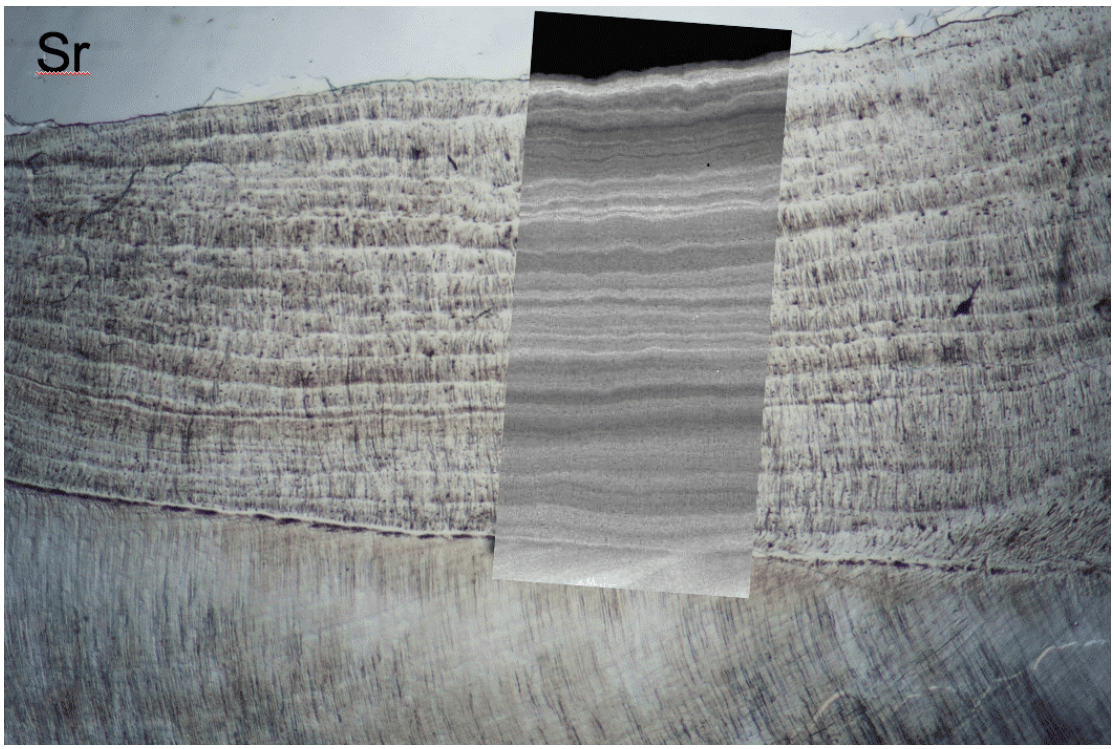

Strontium in *Pan* cellular cementum: Transmission light micrograph of cellular cementum in *Pan* (UCL CA14E LI1) overlain with SXRF map of strontium distribution (5 *μ*m resolution).

Figure S3

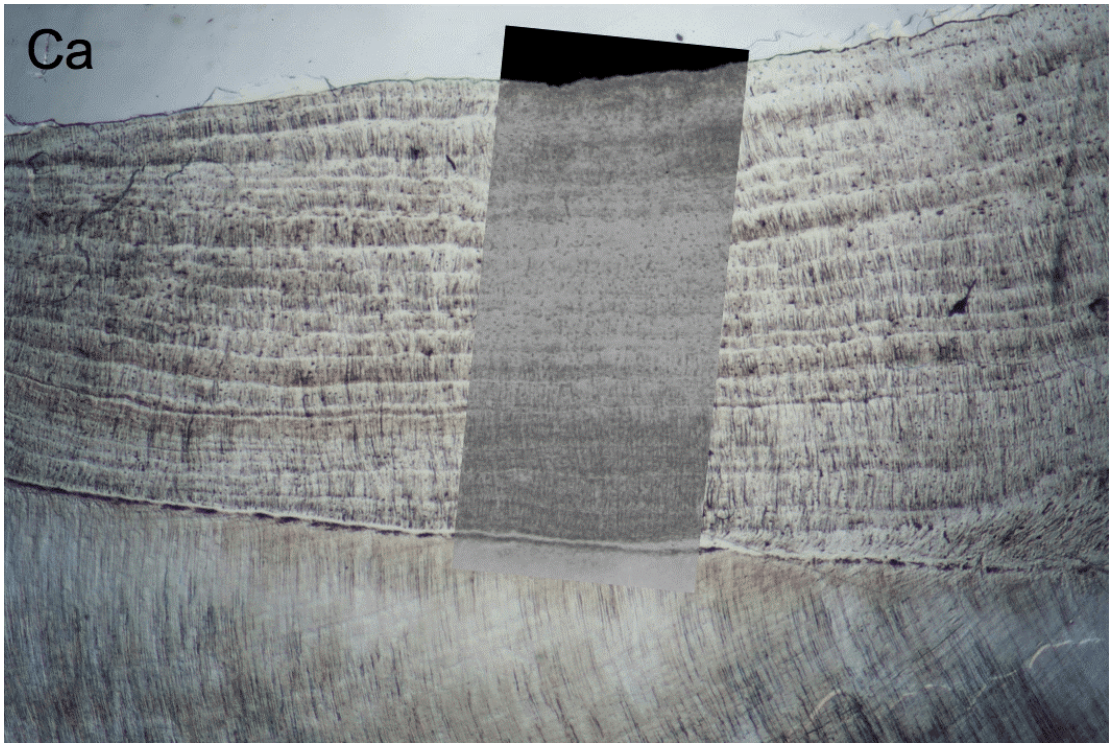

Calcium in *Pan* cellular cementum: Transmission light micrograph of cellular cementum in *Pan* (UCL CA14E LI1) overlain with SXRF map of calcium distribution (5 *μ*m resolution).

Figure S4

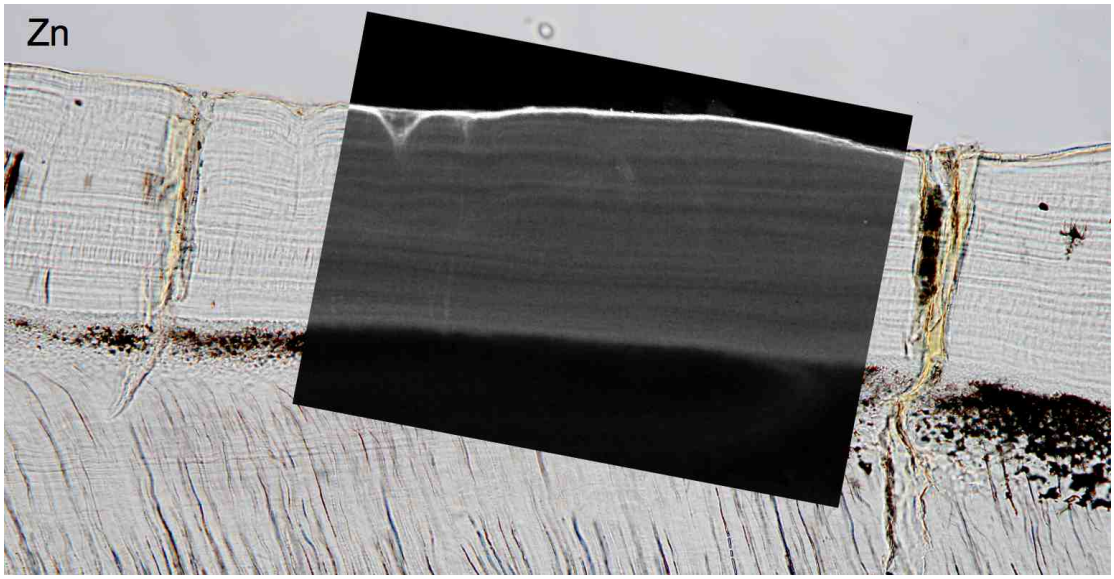

Zinc in *Pongo* acellular cementum: Transmission light micrograph of acellular cementum in *Pongo* (UCL CA 28 I1) overlain with SXRF map of zinc distribution (1 μm resolution).

Figure S5

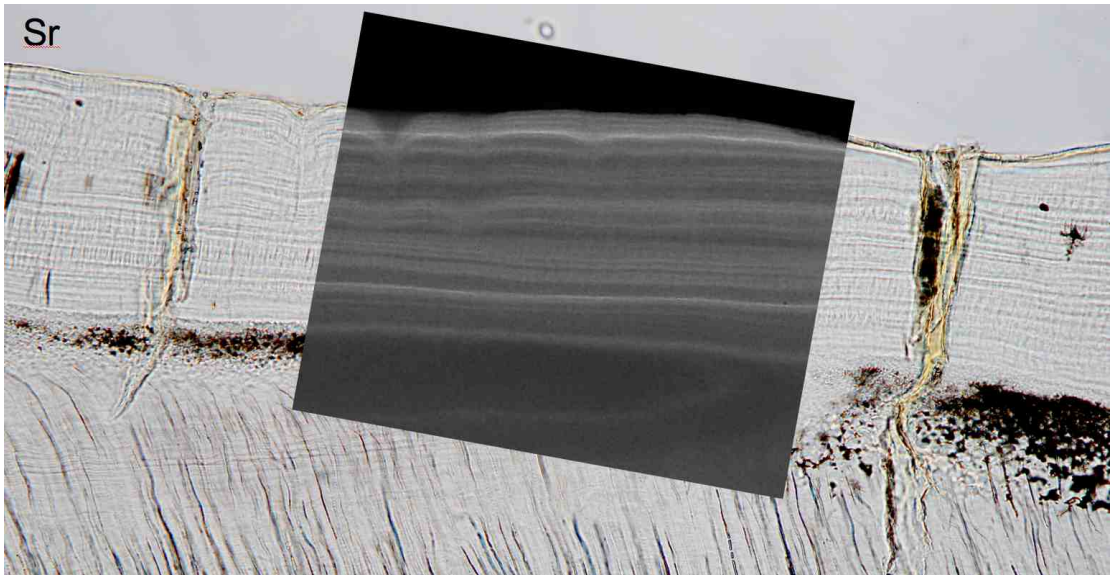

Strontium in *Pongo* acellular cementum: Transmission light micrograph of acellular cementum in *Pongo* (UCL CA 28 I1) overlain with SXRF map of strontium distribution (1 μm resolution).

Figure S6

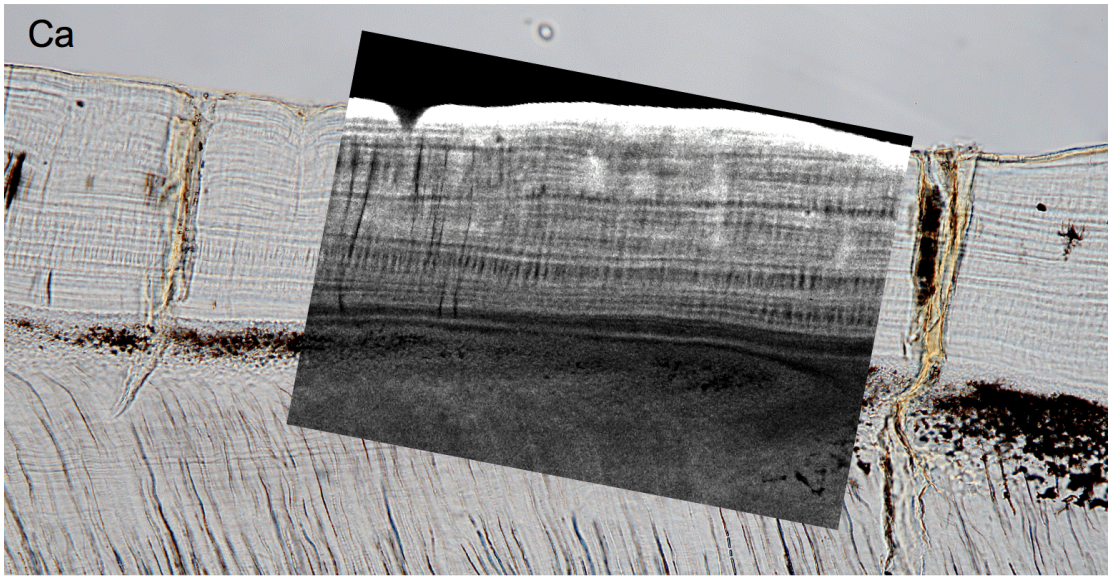

Calcium in *Pongo* acellular cementum: Transmission light micrograph of acellular cementum in *Pongo* (UCL CA 28 I1) overlain with SXRF map of calcium distribution (1 *μ*m resolution).

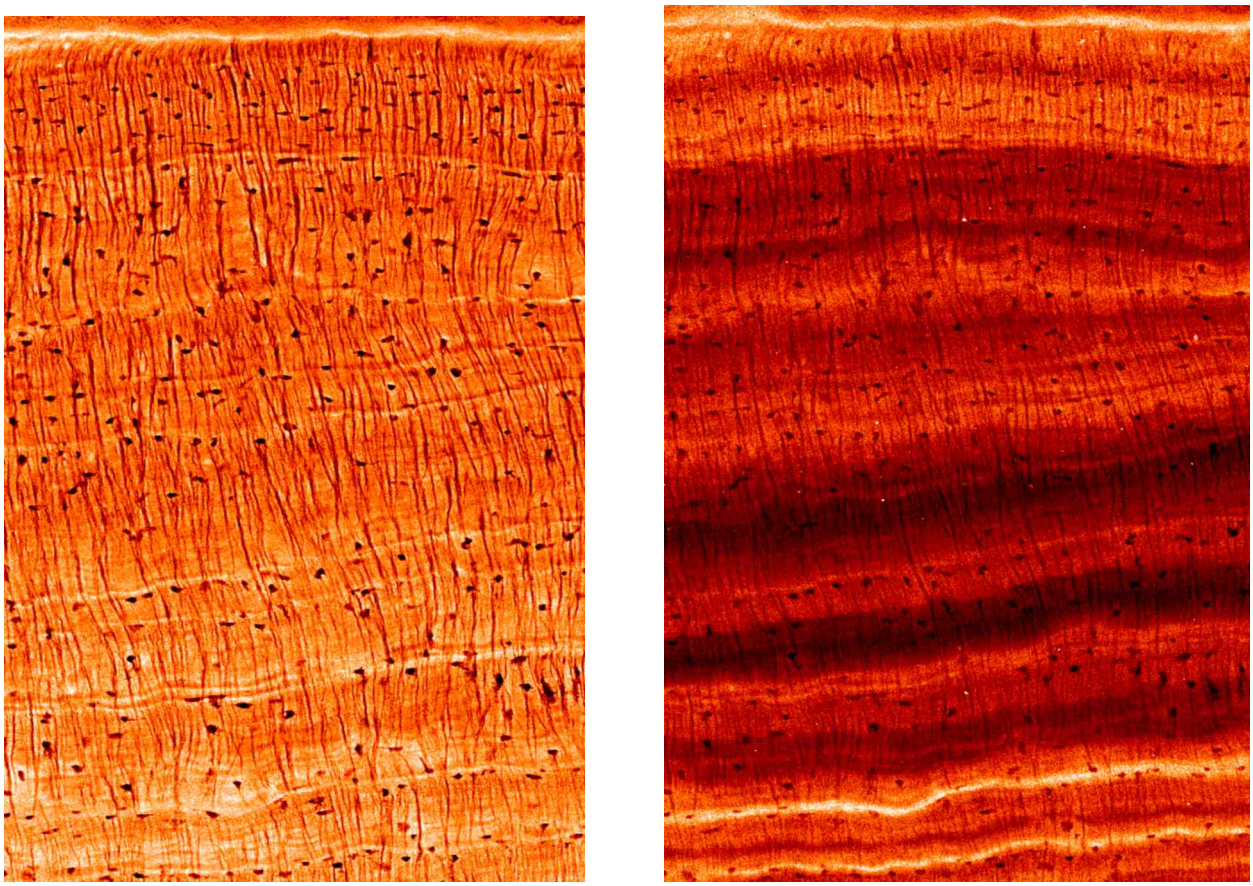

Ca and Sr in *Pan* cellular cementum

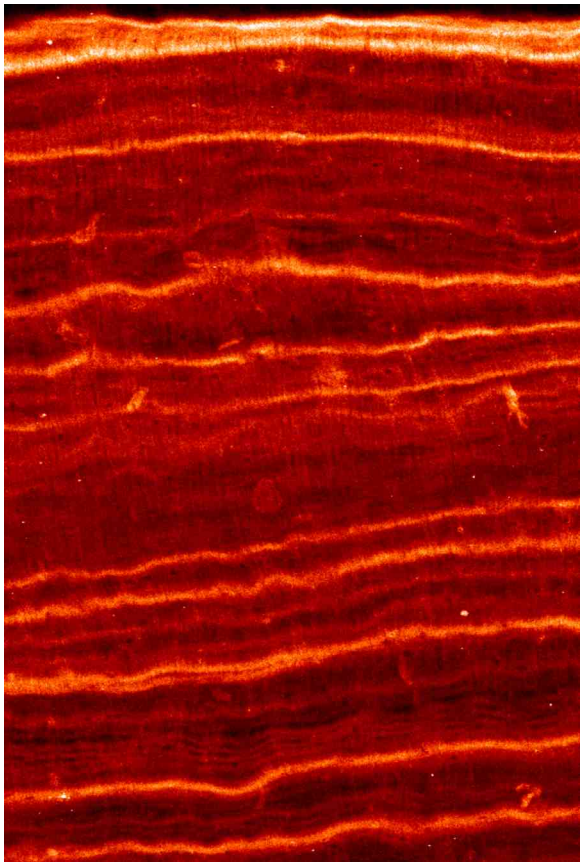

Zn in *Pan* cellular cementum